Dynamical phase diagrams of neural networks with asymmetric couplings

M. N. Tamashiro,* O. Kinouchi,† and S. R. Salinas‡
Instituto de Física, Universidade de São Paulo, Caixa Postal 66318, 05315-970, São Paulo, São Paulo, Brazil
(Received 7 October 1996)

We consider the synchronous updating of a fully connected Ising neural network with separable but asymmetric couplings. In the thermodynamic limit, and away from saturation, it is possible to write a nonlinear mapping for the time evolution of the macroscopic order parameters. A detailed analysis of this mapping is performed for a simple case, with $p=2$ stored patterns. The dynamical phase diagram, in terms of the degree of noise and the parameters of the embedding matrix, displays a rich structure of locked regions into different cycles, in association with nonstandard Farey trees. In some regions of the dynamical phase diagram, we show the coexistence of two different Farey sequences, giving rise to the overlapping of several locked regions. [S1063-651X(97)03504-6]

PACS number(s): 87.10.+e, 05.20.−y, 75.10.Hk

I. INTRODUCTION

The dynamical properties of fully connected Ising neural networks, with separable but asymmetric couplings, have been investigated in a set of papers by Coolen and coworkers [1–4]. The states of the neurons are represented by Ising spin variables that evolve in time according to a stochastic (Glauber) local-field alignment. The separability of the interaction matrix leads to a convenient description in terms of macroscopic variables. Although there is no detailed balance, we can establish a set of (deterministic) equations for the time evolution of the macroscopic order parameters. The attractors of these equations correspond to the stationary solutions of the problem.

In this paper, we look at the simplest, and nontrivial, cases that have not been fully analyzed by previous authors. We consider the synchronous (or parallel) updating of a network with just $p=2$ stored patterns, and a general 2×2 embedding matrix, which leads to a two-dimensional nonlinear mapping for the macroscopic order parameters. It is then feasible to perform detailed calculations to characterize the global dynamical phase diagram of this toy model (in terms of the temperature, which is associated with the level of noise of the system, and the strengths of the symmetric and nonsymmetric components of the embedding matrix). At high temperatures, there is only a trivial (paramagnetic) disordered stable fixed point. At lower levels of noise, there is a rich structure of locked regions (Arnold tongues) into different cycles, depending on the parameters of the embedding matrix. We show that Farey numbers can be used to account for the appearance of these oscillating structures. Although there are also aperiodic limit cycles associated with a vanishing Lyapunov exponent, we have not been able to find chaotic attractors.

The complex structure of the dynamical phase diagrams of these models comes from the competition between symmetric and nonsymmetric contributions to the embedding matrix. The mathematical analogy to the thermodynamic problem of an Ising model with competing ferromagnetic and antiferromagnetic interactions between first and second neighbors along an axial direction (called the ANNNI model [5]) is particularly striking. In the ANNNI model the locked phases are associated with the spatial modulations of the equilibrium magnetization per site along a certain direction. In the neural network models, there is a periodic stationary oscillation in time of the dynamical order parameter. Some analogs of the ANNNI model on a Cayley tree [6] can also be formulated as a nonlinear dissipative mapping that leads to an equally rich and complex phase diagram.

It should be pointed out that asymmetric connection matrices are always closer to biological realism. Also, simple fixed points should not be the rule among the possible attractors of a biologically more realistic dynamical model. Some important phenomena, as the retrieval of temporal sequences and synchronization, can be related to the presence of asymmetric interactions. In the recent literature there are several proposals to use the cyclic attractors of networks with asymmetric interactions to perform a number of computational tasks [7]. Very simple networks, with just a few neurons, have actually been constructed and tested in the laboratory [8]. We hope to provide some illustrations of the general behavior of these models.

This paper is organized as follows. In Sec. II we define the model and write the equations for the time evolution of the macroscopic order parameters. Sections III and IV are dedicated to the detailed analysis of special cases of the model. Some conclusions are presented in Sec. V.

II. DEFINITION OF THE MODEL

We consider a fully connected network of N formal neurons that can be represented by Ising spin variables, $S_i=\pm 1$, for $i=1,\ldots,N$. As usual, $S_i=+1$ indicates that neuron i is firing action potentials at highest rate, and $S_i=-1$ indicates a state of rest. The spins are connected by a synaptic matrix $\{J_{ij}\}$ defined by the separable bilinear Hebbian form,

$$J_{ij}=\frac{1}{N}\sum_{\mu,\nu=1}^{p}\xi_i^\mu A_{\mu\nu}\xi_j^\nu, \tag{1}$$

*Electronic address: mtamashiro@if.usp.br
†Electronic address: osame@gibbs.if.usp.br
‡Electronic address: ssalinas@if.usp.br

for $i \neq j$, and $J_{ii}=0$, where ξ_i^μ, which represents the activity of neuron i in the stored pattern μ, for $\mu=1,...,p$, is a quenched random variable associated with the probability distribution

$$P(\xi_i^\mu)=\tfrac{1}{2}(1+r_\mu)\,\delta(\xi_i^\mu-1)+\tfrac{1}{2}(1-r_\mu)\,\delta(\xi_i^\mu+1). \quad (2)$$

The parameter r_μ, such that $-1<r_\mu<+1$, represents the average activity per neuron in the stored pattern μ. For $A_{\mu\nu}=\delta_{\mu\nu}$ and unbiased patterns ($r_\mu=0$, $\forall\mu$), we regain the Little-Hopfield model [9–11], whose equilibrium properties were investigated in the seminal work of Amit and collaborators [12] (including the case near saturation, for $p=\alpha N$, with finite α [13]).

Although there are some investigations of this class of models with more general forms of the embedding matrix [1–3,14], there is still room for further analysis. The simplest situation, which has not been fully investigated, refers to an attractor neural network with just $p=2$ stored patterns. In this case, the more general 2×2 embedding matrix can be written in the form

$$\mathbf{A}=\begin{pmatrix} 1+a_D & a_S+a_A \\ a_S-a_A & 1-a_D \end{pmatrix}. \quad (3)$$

The diagonal case, $A_{\mu\nu}=\delta_{\mu\nu}$, that is, $a_S=a_A=a_D=0$, for sequential (asynchronous) dynamics corresponds to a spin-glass model proposed by van Hemmen [15]. Coolen and Sherrington [2] have already analyzed the particular case of a symmetric matrix, $a_A=a_D=0$, and Laughton and Coolen [3] have considered the antisymmetric case, $a_S=a_D=0$, for parallel (synchronous) dynamics. In the present paper, we complement these previous studies and explore some features that cannot be observed without considering a generic asymmetry.

To check that Eq. (3) is in fact the more general 2×2 matrix, let us write

$$\widetilde{\mathbf{A}}=\begin{pmatrix} \widetilde{A}_{11} & \widetilde{A}_{12} \\ \widetilde{A}_{21} & \widetilde{A}_{22} \end{pmatrix}=\frac{1}{T}\,\mathbf{A}=\frac{1}{T}\begin{pmatrix} A_{11} & A_{12} \\ A_{21} & A_{22} \end{pmatrix}. \quad (4)$$

The ''pseudotemperature'' T measures the stochasticity of the system. It is related to the (Gaussian) fluctuations of the local fields [9,16], which may come from the random emission of neurotransmitters and the delays on the synapses. We may choose

$$\tfrac{1}{2}\mathrm{Tr}\mathbf{A}=\tfrac{1}{2}(A_{11}+A_{22})=1, \quad (5)$$

that is,

$$\frac{1}{T}=\tfrac{1}{2}\mathrm{Tr}\widetilde{\mathbf{A}}=\tfrac{1}{2}(\widetilde{A}_{11}+\widetilde{A}_{22}). \quad (6)$$

We then see that the embedding matrix can be described in terms of the symmetric (a_S), antisymmetric (a_A), and antidiagonal (a_D) coupling parameters,

$$a_S=\tfrac{1}{2}\ \mathrm{Tr}(\sigma_x\mathbf{A})=\tfrac{1}{2}(A_{12}+A_{21})=\frac{\widetilde{A}_{12}+\widetilde{A}_{21}}{\widetilde{A}_{11}+\widetilde{A}_{22}}, \quad (7)$$

$$a_A=\frac{1}{2i}\ \mathrm{Tr}(\sigma_y\mathbf{A})=\tfrac{1}{2}(A_{12}-A_{21})=\frac{\widetilde{A}_{12}-\widetilde{A}_{21}}{\widetilde{A}_{11}+\widetilde{A}_{22}}, \quad (8)$$

$$a_D=\tfrac{1}{2}\ \mathrm{Tr}(\sigma_z\mathbf{A})=\tfrac{1}{2}(A_{11}-A_{22})=\frac{\widetilde{A}_{11}-\widetilde{A}_{22}}{\widetilde{A}_{11}+\widetilde{A}_{22}}, \quad (9)$$

where σ_x, σ_y, and σ_z are the usual spin-$\frac{1}{2}$ Pauli matrices. This parametrization in terms of these four independent elements, (T,a_S,a_A,a_D), is particularly suitable to exploit the symmetries of the model for unbiased patterns ($r_\mu=0$, $\forall\mu$).

It should be noted that the diagonal Hebbian term, $A_{\mu\nu}=\delta_{\mu\nu}$, gives origin to ordinary point attractors associated with the four patterns, $\pm\boldsymbol{\xi}^1$ and $\pm\boldsymbol{\xi}^2$, corresponding to the Mattis states [17], whereas the remaining terms yield transitions between these patterns. The competition between these conflicting effects leads to a rich dynamical phase diagram in terms of the temperature T and the coupling parameters (a_S,a_A,a_D).

As pointed out in the Introduction, due to the lack of detailed balance, we cannot use the techniques of equilibrium statistical mechanics to analyze models with asymmetric interactions. However, it is still possible to present a dynamical description of the macroscopic behavior. For synchronous updating, we can write the Markov master equation

$$\rho_{n+1}(\mathbf{S})=\sum_{\mathbf{S}'}\ w(\mathbf{S}'\to\mathbf{S})\rho_n(\mathbf{S}'), \quad (10)$$

where $\rho_n(\mathbf{S})$ is the probability of finding the network in the microscopic state $\mathbf{S}=(S_1,\ldots,S_N)$ at discrete time step n, and the transition probability is given by a product of Glauber terms [16],

$$w(\mathbf{S}'\to\mathbf{S})=\prod_{j=1}^{N}\ \tfrac{1}{2}\{1+\tanh[S_j h_j(\mathbf{S}')/T]\}, \quad (11)$$

under the stochastic field

$$h_j(\mathbf{S})=\sum_{k=1}^{N}\ J_{jk}S_k\,. \quad (12)$$

The dynamic macroscopic order parameters are given by the thermal averages of the overlaps between the microscopic states of the network and the stored patterns,

$$m_\mu(n)=\sum_{\mathbf{S}}\ \rho_n(\mathbf{S})\ \frac{1}{N}\sum_{i=1}^{N}\ \xi_i^\mu S_i\,, \quad (13)$$

for $\mu=1,...,p$. If $m_\mu=1$, the μth stored pattern is perfectly retrieved; if $m_\mu=0$, there is no correlation between the network state and the μth stored pattern. The antipattern $-\boldsymbol{\xi}^\mu$ is perfectly retrieved when $m_\mu=-1$. From the master equation, it is easy to show that

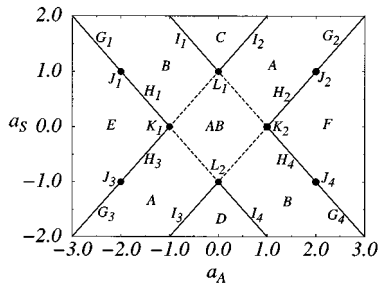

FIG. 1. Ground state at temperature $T=0+$ for $a_D=0$ (the attractors and the associated Farey numbers are given in Table I).

$$m_\mu(n+1)=m_\mu(n)-\frac{2}{N}\sum_{i=1}^{N}\xi_i^\mu\sum_{\mathbf{S}}S_i\rho_n(\mathbf{S})\times\sum_{\mathbf{S}'\neq\mathbf{S}}w(\mathbf{S}\to\mathbf{S}')\delta_{S_i'-S_i}. \tag{14}$$

For a fully connected network with $p=2$, as in the toy model under consideration, the mean-field approximation becomes exact. In the thermodynamic limit, $N\to\infty$, we can then use the properties of self-averaging with respect to the microscopic realizations of the stored patterns to reduce the dynamic process to a one-site problem. The temporal evolution of the dynamical order parameters is finally written as a set of difference equations,

$$m_\gamma(n+1)=\left\langle \xi_i^\gamma\tanh\left[\frac{1}{T}\sum_{\mu,\nu=1}^{p}\xi_i^\mu A_{\mu\nu}m_\nu(n)\right]\right\rangle_{\boldsymbol{\xi}}, \tag{15}$$

where the angular brackets denote an average with respect to the probability distribution (2) of the stored patterns.

For the toy model ($p=2$), Eq. (15) can be written in the explicit form

$$\begin{pmatrix}m_1(n+1)\\ m_2(n+1)\end{pmatrix}=\frac{1+r_1r_2}{2}\begin{pmatrix}1\\1\end{pmatrix}\tanh\left\{\frac{1}{T}[(1+a_S-a_A+a_D)\times m_1(n)+(1+a_S+a_A-a_D)m_2(n)]\right\}+\frac{1-r_1r_2}{2}\begin{pmatrix}1\\-1\end{pmatrix}\tanh\left\{\frac{1}{T}[(1-a_S+a_A+a_D)m_1(n)-(1-a_S-a_A-a_D)m_2(n)]\right\}. \tag{16}$$

Although starting from more realistic learning rules, it is remarkable that Peretto [18] has obtained an analogous set of (differential) equations for the asynchronous updating of unbiased patterns.

Introducing the variables

$$x_n=\frac{1}{1+r_1r_2}[m_1(n)+m_2(n)], \tag{17}$$

and

$$y_n=\frac{1}{1-r_1r_2}[m_1(n)-m_2(n)], \tag{18}$$

TABLE I. Different regions in the ground state at $T=0+$ for $a_D=0$.

A	=	$\begin{matrix}+\\+\end{matrix}$	and	$\begin{matrix}-\\-\end{matrix}$	(0/2)					
B	=	$\begin{matrix}+\\-\end{matrix}$	and	$\begin{matrix}-\\+\end{matrix}$	(0/2)					
C	=	$\begin{matrix}+&+\\+&-\end{matrix}$	and	$\begin{matrix}-&-\\+&-\end{matrix}$	(2/4)					
D	=	$\begin{matrix}+&-\\+&+\end{matrix}$	and	$\begin{matrix}+&-\\-&-\end{matrix}$	(2/4)					
E	=	$\begin{matrix}+&+&-&-\\+&-&-&+\end{matrix}$			(1/4)					
F	=	$\begin{matrix}+&+&-&-\\-&+&+&-\end{matrix}$			(1/4)					
G_1	=	$\begin{matrix}-&0&+&0\\+&+&-&-\end{matrix}$			(1/4)					
G_2	=	$\begin{matrix}+&0&-&0\\+&+&-&-\end{matrix}$			(1/4)					
G_3	=	$\begin{matrix}+&+&-&-\\+&0&-&0\end{matrix}$			(1/4)					
G_4	=	$\begin{matrix}+&+&-&-\\-&0&+&0\end{matrix}$			(1/4)					
H_1	=	$\begin{matrix}-&0&+&+&0&-\\+&+&+&-&-&-\end{matrix}$						(1/6)		
H_2	=	$\begin{matrix}+&0&-&-&0&+\\+&+&+&-&-&-\end{matrix}$						(1/6)		
H_3	=	$\begin{matrix}+&+&+&-&-&-\\+&0&-&-&0&+\end{matrix}$						(1/6)		
H_4	=	$\begin{matrix}+&+&+&-&-&-\\-&0&+&+&0&-\end{matrix}$						(1/6)		
I_1	=	$\begin{matrix}+&+\\-&0\end{matrix}$	and	$\begin{matrix}-&-\\+&0\end{matrix}$	(2/4)					
I_2	=	$\begin{matrix}+&+\\+&0\end{matrix}$	and	$\begin{matrix}-&-\\-&0\end{matrix}$	(2/4)					
I_3	=	$\begin{matrix}+&0\\+&+\end{matrix}$	and	$\begin{matrix}-&0\\-&-\end{matrix}$	(2/4)					
I_4	=	$\begin{matrix}-&0\\+&+\end{matrix}$	and	$\begin{matrix}+&0\\-&-\end{matrix}$	(2/4)					
J_1	=	$\begin{matrix}+&+&0&-&-&0\\0&-&-&0&+&+\end{matrix}$						(1/6)		
J_2	=	$\begin{matrix}+&+&0&-&-&0\\0&+&+&0&-&-\end{matrix}$						(1/6)		
J_3	=	$\begin{matrix}0&+&+&0&-&-\\+&+&0&-&-&0\end{matrix}$						(1/6)		
J_4	=	$\begin{matrix}0&-&-&0&+&+\\+&+&0&-&-&0\end{matrix}$						(1/6)		
K_1	=	$\begin{matrix}+&+&+&0&-&-&-&0\\+&0&-&-&-&0&+&+\end{matrix}$								(1/8)
K_2	=	$\begin{matrix}+&+&+&0&-&-&-&0\\-&0&+&+&+&0&-&-\end{matrix}$								(1/8)
L_1	=	$\begin{matrix}+\\0\end{matrix}$	and	$\begin{matrix}-\\0\end{matrix}$	(0/2)					
L_2	=	$\begin{matrix}0\\+\end{matrix}$	and	$\begin{matrix}0\\-\end{matrix}$	(0/2)					

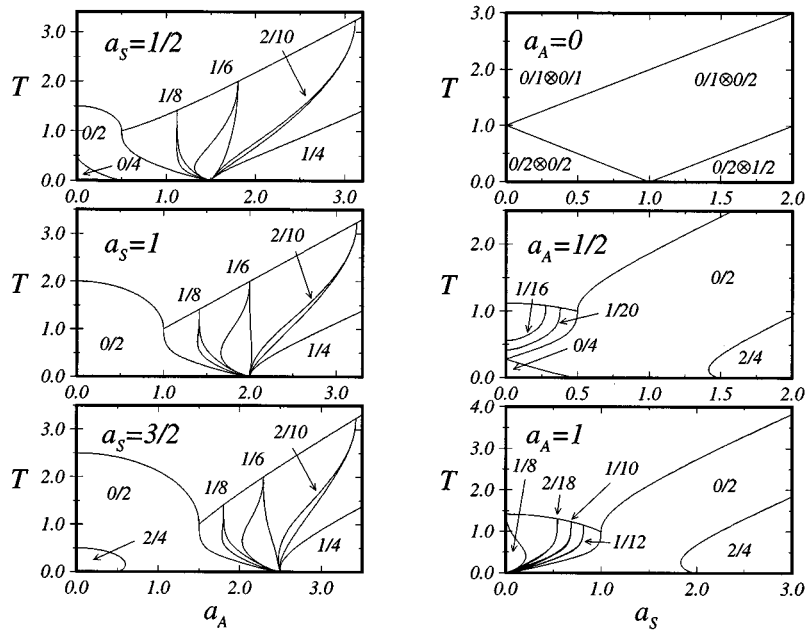

FIG. 2. Dynamical phase diagrams for $a_D=0$, $T>0$, and some typical values of the parameters a_S and a_A. Only the widest mode-locked regions are displayed. The various attractors are labeled by the corresponding Farey numbers.

we can also write

$$x_{n+1}=\tanh\left\{\frac{1}{T}\left[(1+r_1r_2)(1+a_S)x_n+(1-r_1r_2)(a_D-a_A)y_n\right]\right\},$$

$$y_{n+1}=\tanh\left\{\frac{1}{T}\left[(1+r_1r_2)(a_D+a_A)x_n+(1-r_1r_2)(1-a_S)y_n\right]\right\}, \tag{19}$$

which can be symbolically represented as

$$\mathbf{x}_{n+1}=\mathbf{F}(\mathbf{x}_n), \tag{20}$$

where $\mathbf{x}_n=(x_n,y_n)$.

To analyze the linear stability of the attractors of the mapping, we define the Lyapunov exponents $\{\lambda_\mu\}$, which measure the mean exponential rate of convergence or divergence of trajectories surrounding the attractor,

$$\lambda_\mu=\lim_{M\to\infty}\frac{1}{M}\ln|\Lambda_\mu| \quad (\mu=1,2), \tag{21}$$

where $\{\Lambda_\mu\}$ are the eigenvalues of the product matrix

$$\mathbf{J}(\mathbf{x}_M)\mathbf{J}(\mathbf{x}_{M-1})\cdots\mathbf{J}(x_2)\mathbf{J}(\mathbf{x}_1), \tag{22}$$

formed by the product of the Jacobian matrices

$$\mathbf{J}(\mathbf{x}_n)=\frac{\partial(x_{n+1},y_{n+1})}{\partial(x_n,y_n)}=\begin{pmatrix}\frac{\partial x_{n+1}}{\partial x_n} & \frac{\partial x_{n+1}}{\partial y_n}\\ \frac{\partial y_{n+1}}{\partial x_n} & \frac{\partial y_{n+1}}{\partial y_n}\end{pmatrix}=\frac{1}{T}\begin{pmatrix}(1+r_1r_2)(1+a_S)(1-x_{n+1}^2) & (1-r_1r_2)(a_D-a_A)(1-x_{n+1}^2)\\ (1+r_1r_2)(a_D+a_A)(1-y_{n+1}^2) & (1-r_1r_2)(1-a_S)(1-y_{n+1}^2)\end{pmatrix}, \tag{23}$$

computed along the attractor.

As the hyperbolic tangent is an odd function of its argument, the analysis of the mapping for $T>0$ can be easily extended to $T<0$. The attractors of these two cases are related by the following transformations: (i) if $\mathbf{x}^*$ is a stable fixed point of the mapping for $T>0$, we have a stable two-cycle given by $\{\mathbf{x}^*,-\mathbf{x}^*\}$ for $T<0$; (ii) if $\{\mathbf{x}_1^*,\mathbf{x}_2^*,\mathbf{x}_{Q-1}^*,\mathbf{x}_Q^*\}$ is a periodic cycle of period Q (odd) for $T>0$, we have a periodic cycle of period $2Q$ for $T<0$, defined by $\{\mathbf{x}_1^*,-\mathbf{x}_2^*,\ldots,(-1)^{k+1}\mathbf{x}_k^*,\ldots,\mathbf{x}_Q^*,-\mathbf{x}_1^*,\mathbf{x}_2^*,\ldots,(-1)^k\mathbf{x}_k^*,\ldots,-\mathbf{x}_Q^*\}$, where $k\in\{1,\ldots,Q\}$; (iii) if $\{\mathbf{x}_1^*,\mathbf{x}_2^*,\ldots,\mathbf{x}_{Q-1}^*,\mathbf{x}_Q^*\}$ is a periodic cycle of period Q (even) for $T>0$, we have a periodic cycle of period Q for $T<0$, defined by $\{\mathbf{x}_1^*,-\mathbf{x}_2^*,\ldots,(-1)^{k+1}\mathbf{x}_k^*,\ldots,-\mathbf{x}_Q^*\}$, where $k\in\{1,\ldots,Q\}$.

We remark that Eq. (19) corresponds to a subspace of the more general class of mappings,

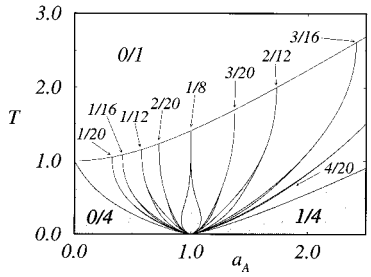

FIG. 3. Dynamical phase diagram for $a_S=a_D=0$ and $T>0$. The more important tongues are labeled by the corresponding Farey numbers. The Farey numbers of the $T<0$ dynamical phase diagram are obtained by the generating numbers 2/4 and 1/4.

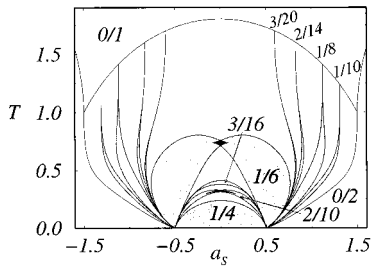

FIG. 4. Dynamical phase diagram for $a_A=\frac{3}{2}$, $a_D=0$, and $T>0$. In the darker shaded regions there is a costability of periodic attractors with the same winding numbers, but different structures (see the magnifications in Fig. 5).

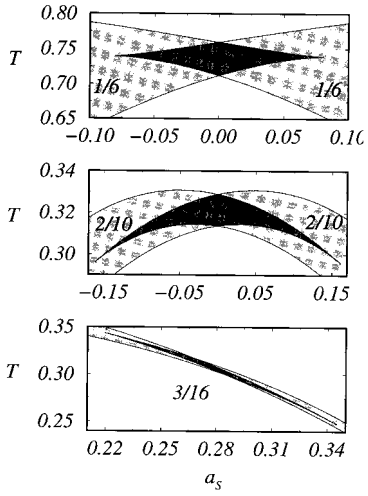

FIG. 5. Magnifications of some costability regions of the dynamical phase diagram for $a_A=\frac{3}{2}$, $a_D=0$, and $T>0$. The attractors are labeled by the corresponding Farey numbers. In the darker shaded regions there is a costability of periodic attractors with the same winding numbers, but different structures.

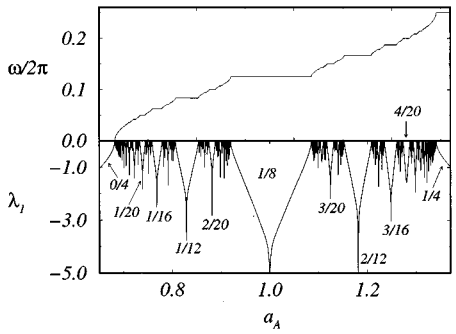

FIG. 6. Devil's staircase ($\omega/2\pi$ versus a_A) associated with the winding numbers of the Arnold tongues and the corresponding largest Lyapunov exponent (λ_1 versus a_A) for $a_S=a_D=0$ and $T=0.15$. The devil's staircase for $T=-0.15$ is obtained by reflection around $\omega/2\pi=1/4$.

$$X_{n+1}=g(w_{11}X_n+w_{12}Y_n+\theta_X),$$

$$Y_{n+1}=g(w_{21}X_n+w_{22}Y_n+\theta_Y), \tag{24}$$

with

$$g(h)=c_1+c_2\tanh(\gamma h), \tag{25}$$

which describe two coupled sigmoidal neurons with self-couplings (w_{11} and w_{22}) and threshold terms (θ_X and θ_Y). The case $c_1=c_2=\gamma=\frac{1}{2}$, that is, $g(h)=(1+e^{-h})^{-1}$, has been considered by Pasemann and Nelle [19]. In this particular case, with a suitable change of variables, $\mathbf{x}_n=2\mathbf{X}_n-1$, and with the redefinitions

$$\frac{1}{T}(1+a_S)=\tfrac{1}{4}w_{11},$$

$$\frac{1}{T}(a_D-a_A)=\tfrac{1}{4}w_{12},$$

$$\frac{1}{T}H_x=\tfrac{1}{2}(\theta_X+\tfrac{1}{2}w_{11}+\tfrac{1}{2}w_{12}),$$

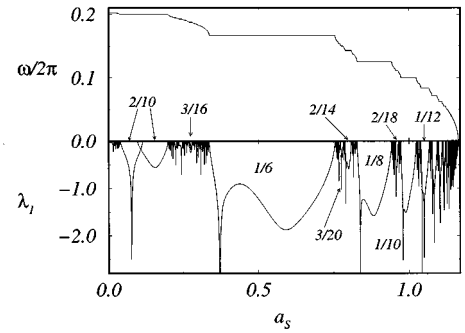

FIG. 7. Devil's staircase ($\omega/2\pi$ versus a_S) associated with the winding numbers of the Arnold tongues and the corresponding largest Lyapunov exponent (λ_1 versus a_S) for $a_A=\frac{3}{2}$, $a_D=0$, and $T=0.31$. The devil's staircase for $T=-0.31$ is obtained by reflection around $\omega/2\pi=1/4$.

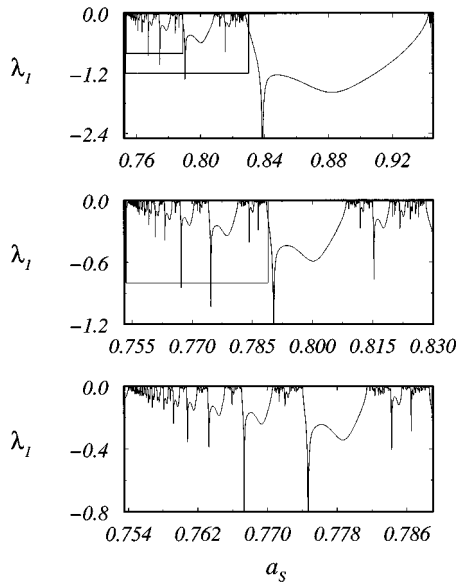

FIG. 8. Largest Lyapunov exponent (λ_1 versus a_S) for $a_A=\frac{3}{2}$, $a_D=0$, and $T=0.31$. These graphs represent several magnifications of the lower portion of Fig. 7 to allow a better view of the presumed fractal structure. The magnified regions are bounded by rectangles.

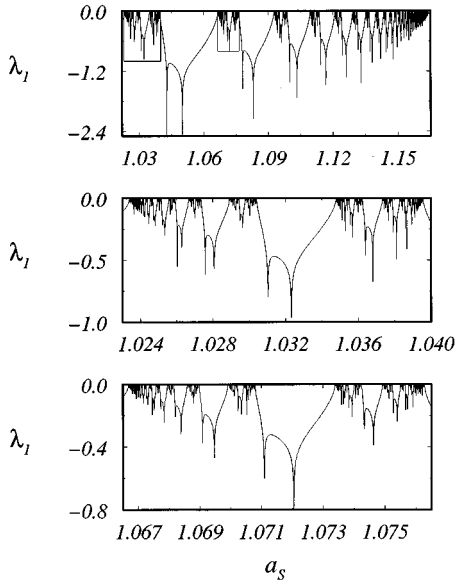

FIG. 9. Largest Lyapunov exponent (λ_1 versus a_S) for $a_A=\frac{3}{2}$, $a_D=0$, and $T=0.31$. These graphs represent several magnifications of the lower portion of Fig. 7 to allow a better view of the presumed fractal structure. The magnified regions are bounded by rectangles.

$$\frac{1}{T}(1-a_S)=\tfrac{1}{4}w_{22},$$

$$\frac{1}{T}(a_D+a_A)=\tfrac{1}{4}w_{21},$$

$$\frac{1}{T}H_y=\tfrac{1}{2}(\theta_Y+\tfrac{1}{2}w_{22}+\tfrac{1}{2}w_{21}),$$

the mapping (24) can be written as in Eq. (19) for unbiased patterns with the inclusion of the additional thresholds H_x and H_y. For this model, Stollenwerk and Pasemann [20] have detected the existence of strange attractors in a region of the dynamical phase diagram near the parameters $T=-\frac{2}{5}$, $a_s=1$, $a_A=\frac{3}{5}$, $a_D=0$, $H_x=\frac{9}{5}$, and $H_y=0$.

III. ANALYSIS OF THE MAPPING FOR $a_D=0$ AND UNBIASED PATTERNS

In the absence of antidiagonal couplings ($a_D=0$) and for unbiased patterns ($r_1=r_2=0$), besides the trivial symmetry by inversion, $(x,y)\rightarrow(-x,-y)$, the mapping is also invariant by inversion of the coupling parameters a_S and a_A together with the coordinate transformations

$$(x,y)\rightarrow(y,-x) \quad \text{if} \quad a_S\rightarrow -a_S \tag{26}$$

and

$$(x,y)\rightarrow(x,-y) \quad \text{if } a_A\rightarrow -a_A. \tag{27}$$

The dynamical phase diagrams will be symmetric in the $a_S\times a_A$ subspace of parameters. Furthermore, due to the additional symmetry by temperature inversion, $T\rightarrow -T$, it is sufficient to obtain the phase diagram in the first octant of the three-dimensional parameter space, (T,a_S,a_A).

In Fig. 1, we show the ground state (at $T\rightarrow 0+$). The indexed letters in this phase diagram refer to attractors represented in the form

$$\begin{pmatrix} x_1^*\cdots x_Q^* \\ y_1^*\cdots y_Q^* \end{pmatrix}.$$

The different regions, together with the respective Farey numbers, are explicitly given in Table I. To make contact with the analysis of Coolen and Sherrington [2], we identify the simplest states: (i) A and B are Mattis regions (patterns 1 and 2, respectively); (ii) L_1 and L_2 are points of spurious or mixture states; (iii) regions C and D are associated with cyclic structures. In region AB (which we call Hopfield region), there is a costability of states A and B. Mixed states occur for $a_A=0$ only (due to the uncoupling of the mapping in this particular case).

The usual methods of the theory of bifurcations [21] can be used to obtain the dynamical phase diagrams for nonvan-

TABLE II. Farey hierarchy for smaller values of a_S.

$n=0$	$\rightarrow$	$\frac{0}{4}$																		$\frac{1}{4}$
$n=1$	$\rightarrow$											$\frac{1}{8}$								
$n=2$	$\rightarrow$					$\frac{1}{12}$										$\frac{2}{12}$				
$n=3$	$\rightarrow$			$\frac{1}{16}$				$\frac{2}{20}$					$\frac{3}{20}$					$\frac{3}{16}$		
$n=4$	$\rightarrow$		$\frac{1}{20}$		$\frac{2}{28}$		$\frac{3}{32}$		$\frac{3}{28}$		$\frac{4}{28}$			$\frac{5}{32}$			$\frac{5}{28}$		$\frac{4}{20}$	

TABLE III. Farey hierarchy for larger values of a_S.

$n=0$	$\rightarrow$	$\frac{0}{2}$																						$\frac{1}{4}$
$n=1$	$\rightarrow$												$\frac{1}{6}$											
$n=2$	$\rightarrow$					$\frac{1}{8}$											$\frac{2}{10}$							
$n=3$	$\rightarrow$			$\frac{1}{10}$				$\frac{2}{14}$						$\frac{3}{16}$						$\frac{3}{14}$				
$n=4$	$\rightarrow$		$\frac{1}{12}$		$\frac{2}{18}$		$\frac{3}{22}$		$\frac{3}{20}$		$\frac{4}{22}$		$\frac{5}{26}$			$\frac{5}{24}$			$\frac{4}{18}$					

ishing temperatures. At the trivial (paramagnetic) disordered fixed point, $\mathbf{x}^*=(x^*,y^*)=(0,0)$, the eigenvalues of the Jacobian matrix can be written in closed form,

$$\Lambda_{1,2}=\frac{1}{T}\pm\frac{1}{T}\sqrt{a_S^2-a_A^2}. \tag{28}$$

We should consider two cases.

(i) For $|a_S|>|a_A|$, these eigenvalues are real. The system may undergo either a supercritical pitchfork bifurcation (for $T>0$) or a period-doubling (or flip) bifurcation (for $T<0$) at the critical temperature

$$|T_c|=1+\sqrt{a_S^2-a_A^2}. \tag{29}$$

The continuous transitions are between the disordered (paramagnetic) state and either the Mattis (ferromagnetic) states, for $T>0$, or a cyclic (antiferromagnetic) state, for $T<0$. The disordered state is characterized by the Farey number 0/1, whereas the ordered states are associated with the Farey numbers 0/2, for $T>0$, or 1/2, for $T<0$, respectively.

(ii) For $|a_S|<|a_A|$, the eigenvalues are complex conjugates. The system undergoes a Hopf supercritical bifurcation at the critical temperature

$$|T_c|=\sqrt{1+a_A^2-a_S^2}, \tag{30}$$

associated with a continuous transition between the disordered state and a periodic cycle with a critical winding number ω_c ($0\leq\omega_c\leq\pi/2$, for $T_c>0$; $\pi/2\leq\omega_c\leq\pi$, for $T_c<0$) that satisfies the relations

$$\cos\omega_c=\frac{1}{T_c} \tag{31}$$

and

$$\tan\omega_c=[a_A^2-a_S^2]^{1/2}. \tag{32}$$

From Eqs. (29) and (30), we obtain the stability borders of the trivial disordered state. The stability borders of the periodic cycles and of the attractive fixed points, corresponding to the Mattis states, are determined from the largest associated Lyapunov exponents (see the phase diagrams in Figs. 2–5; note that we are indicating the main periodic regions only).

The two-dimensional nonlinear mapping given by Eq. (20) presents synchronization (phase-locking) associated with Arnold tongues. There are finite regions of the dynamical phase diagram where the period of a given cycle remains locked, giving rise to a devil's staircase structure in terms of the winding number. Figures 6 and 7 display this devil's staircase structure (with the associated largest Lyapunov exponent) for two distinct sections of the dynamical phase diagram. As in the case of the analogs of the ANNNI model on a Cayley tree, the devil's staircases are expected to display a fractal nature. It is peculiar to see that the Lyapunov exponents themselves seem to exhibit this same kind of fractal behavior. In Figs. 8 and 9 we illustrate the presumed fractal character of the largest Lyapunov exponent.

The winding number associated with an Arnold tongue can be written as a rational $\omega/2\pi=P/Q$, where P and Q are relative prime integers (Q is the period of the cycle and P is the number of minima within that period; ω represents an ''average'' angular frequency). The structure of the Arnold tongues in the dynamical phase diagram is described by a *Farey hierarchy* [22]. In a *standard* Farey hierarchy, the Farey number coincides with the winding number. Given the two widest Arnold tongues labeled by the Farey numbers P_1/Q_1 and P_2/Q_2, the next Farey number (which labels the next widest Arnold tongue), is obtained by the composition rule

$$\frac{P}{Q}=\frac{P_1+P_2}{Q_1+Q_2}. \tag{33}$$

This procedure creates a hierarchical tree, whose elements are obtained from the ratio between the sums of the numerators and the denominators of the preceding Farey numbers. The horizontal ordering of the Farey numbers gives the relative position of the Arnold tongues in the dynamical phase diagram, whereas the vertical ordering, hierarchically structured, yields a qualitative indication of the region occupied by the various Arnold tongues. Arnold tongues identified by Farey numbers at the top are wider than tongues identified by numbers at the bottom of the hierarchy.

In *standard* Farey hierarchies, the generating fractions P_1/Q_1 and P_2/Q_2 produce Farey numbers such that P and Q are always relative primes (that is, the winding and the Farey numbers coincide). In *nonstandard* Farey hierarchies [23], however, P and Q may have some common factor (as $m\times P$ and $m\times Q$). In this nonstandard case, the Farey numbers,

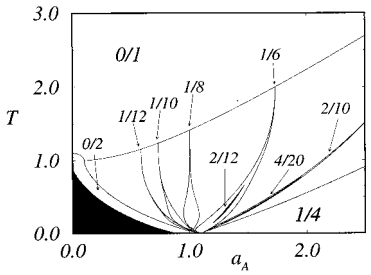

FIG. 10. Dynamical phase diagram for $a_S=0.1$, $a_D=0$, and $T>0$. Notice the complex coexistence of two distinct Farey structures, giving rise to the overlapping of several Arnold tongues and internal costability regions for some periodic stationary states.

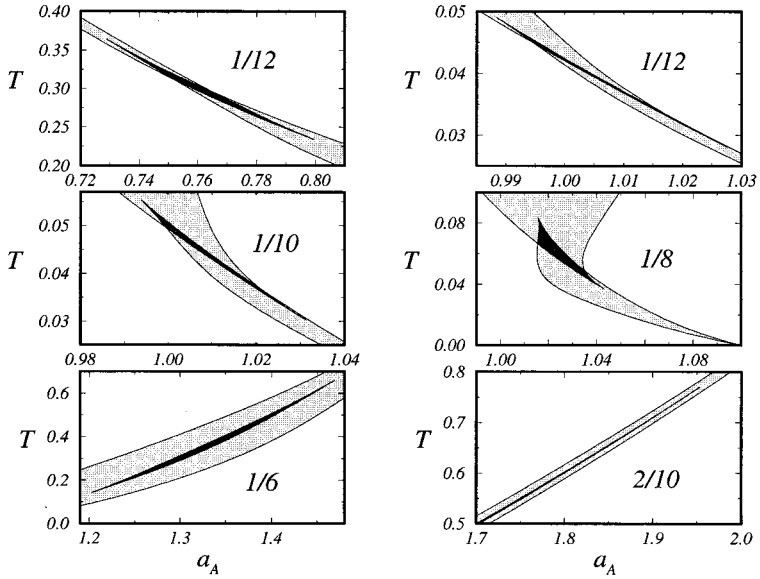

FIG. 11. Magnifications of some costability regions of the dynamical phase diagram for $a_S=0.1$, $a_D=0$, and $T>0$. The attractors are labeled by the corresponding Farey numbers. In the darker shaded regions, some of them very slim, there is a costability of periodic attractors with the same winding numbers, but different structures.

which are written as a reducible fraction of the form $(m\times P)/(m\times Q)$, do not coincide with the winding numbers; they just indicate the costability of m attractors with the same winding number P/Q.

In the present situation ($a_D=0$ and $T>0$), we have two distinct Farey hierarchies. For smaller values of a_S the generating numbers of the hierarchy are given by the fractions 0/4 ($m=4$, $P/Q=0/1$, that is, there are four costable fixed points) and 1/4 (a four cycle), as shown in Table II. For larger values of a_S the generating fractions are 0/2 (two costable fixed points) and 1/4 (a four cycle), as shown in Table III. For intermediate values of a_S these two distinct Farey hierarchies coexist, as we can see in Figs. 10 and 11. Note the complex coexistence of two distinct Farey structures giving rise to the overlap of several Arnold tongues and the internal costability regions for some periodic stationary states. To allow a better appreciation of these details, we show some magnifications of the phase diagram in Fig. 11. In the darker shaded regions, some of them very slim, there is a costability of periodic attractors with the same winding numbers, but different structures. For $T<0$, the structures are generated by the Farey numbers 2/4 and 1/4 (for smaller values of a_S) and 1/2 and 1/4 (for larger values of a_S).

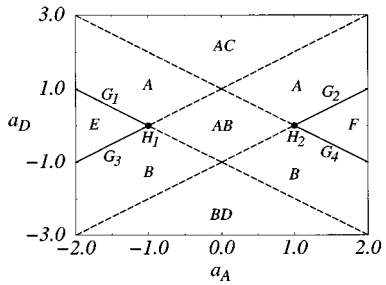

FIG. 12. Ground state at temperature $T=0+$ for $a_S=0$ (the attractors and the associated Farey numbers are given in Table IV).

IV. ANALYSIS OF THE MAPPING FOR $a_S=0$ AND UNBIASED PATTERNS

The complexity of the dynamical phase diagrams is not a particular property of the $a_D=0$ subspace. Even for an antisymmetric embedding matrix ($a_S=0$) in the presence of antidiagonal elements ($a_D\neq 0$), we obtain the same kind of generic behavior as shown in the Sec. III. Besides the trivial symmetry by inversion, $(x,y)\rightarrow(-x,-y)$, the mapping is invariant by inversion of the coupling parameters a_A and a_D together with the coordinate transformations

$$(x,y)\rightarrow(y,x) \quad \text{if} \quad a_A\rightarrow -a_A \tag{34}$$

and

$$(x,y)\rightarrow(y,-x) \quad \text{if} \quad a_D\rightarrow -a_D\,. \tag{35}$$

The dynamical phase diagrams will be symmetric in the subspace of parameters $a_A\times a_D$. Furthermore, due to the additional symmetry by temperature inversion, $T\rightarrow -T$, it is sufficient to consider the phase diagrams in the first octant of the three-dimensional parameter space, (T,a_A,a_D).

In Fig. 12 we show the ground state for $T=0+$. As in Fig. 1, the indexed letters refer to attractors in the form

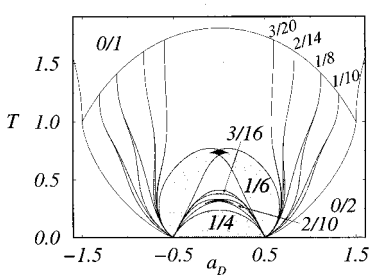

FIG. 13. Dynamical phase diagram for $a_A=\frac{3}{2}$, $a_S=0$, and $T>0$. In the darker shaded regions there is a costability of periodic attractors with the same winding numbers, but different structures. Notice the similarity of this figure with the dynamical phase diagram obtained for $a_A=3/2$ and $a_D=0$, given by Fig. 4.

TABLE IV. Different regions in the ground state at $T=0+$ for $a_S=0$.

A	=	$\begin{matrix}+\\+\end{matrix}$	and	$\begin{matrix}-\\-\end{matrix}$	(0/2)					
B	=	$\begin{matrix}+\\-\end{matrix}$	and	$\begin{matrix}-\\+\end{matrix}$	(0/2)					
C	=	$\begin{matrix}+\\-\end{matrix}$	$\begin{matrix}-\\+\end{matrix}$	(1/2)						
D	=	$\begin{matrix}+\\+\end{matrix}$	$\begin{matrix}-\\-\end{matrix}$	(1/2)						
E	=	$\begin{matrix}+\\+\end{matrix}$	$\begin{matrix}+\\-\end{matrix}$	$\begin{matrix}-\\-\end{matrix}$	$\begin{matrix}-\\+\end{matrix}$	(1/4)				
F	=	$\begin{matrix}+\\-\end{matrix}$	$\begin{matrix}+\\+\end{matrix}$	$\begin{matrix}-\\+\end{matrix}$	$\begin{matrix}-\\-\end{matrix}$	(1/4)				
G_1	=	$\begin{matrix}+\\+\end{matrix}$	$\begin{matrix}+\\0\end{matrix}$	$\begin{matrix}+\\-\end{matrix}$	$\begin{matrix}-\\-\end{matrix}$	$\begin{matrix}-\\0\end{matrix}$	$\begin{matrix}-\\+\end{matrix}$	(1/6)		
G_2	=	$\begin{matrix}+\\+\end{matrix}$	$\begin{matrix}0\\+\end{matrix}$	$\begin{matrix}-\\+\end{matrix}$	$\begin{matrix}-\\-\end{matrix}$	$\begin{matrix}0\\-\end{matrix}$	$\begin{matrix}+\\-\end{matrix}$	(1/6)		
G_3	=	$\begin{matrix}-\\+\end{matrix}$	$\begin{matrix}0\\+\end{matrix}$	$\begin{matrix}+\\+\end{matrix}$	$\begin{matrix}+\\-\end{matrix}$	$\begin{matrix}0\\-\end{matrix}$	$\begin{matrix}-\\-\end{matrix}$	(1/6)		
G_4	=	$\begin{matrix}+\\-\end{matrix}$	$\begin{matrix}+\\0\end{matrix}$	$\begin{matrix}+\\+\end{matrix}$	$\begin{matrix}-\\+\end{matrix}$	$\begin{matrix}-\\0\end{matrix}$	$\begin{matrix}-\\-\end{matrix}$	(1/6)		
H_1	=	$\begin{matrix}+\\+\end{matrix}$	$\begin{matrix}+\\0\end{matrix}$	$\begin{matrix}+\\-\end{matrix}$	$\begin{matrix}0\\-\end{matrix}$	$\begin{matrix}-\\-\end{matrix}$	$\begin{matrix}-\\0\end{matrix}$	$\begin{matrix}-\\+\end{matrix}$	$\begin{matrix}0\\+\end{matrix}$	(1/8)
H_2	=	$\begin{matrix}+\\-\end{matrix}$	$\begin{matrix}+\\0\end{matrix}$	$\begin{matrix}+\\+\end{matrix}$	$\begin{matrix}0\\+\end{matrix}$	$\begin{matrix}-\\+\end{matrix}$	$\begin{matrix}-\\0\end{matrix}$	$\begin{matrix}-\\-\end{matrix}$	$\begin{matrix}0\\-\end{matrix}$	(1/8)

$$\begin{pmatrix} x_1^* \cdots x_Q^* \\ y_1^* \cdots y_Q^* \end{pmatrix}.$$

The different regions, together with the respective Farey numbers, are explicitly given in Table IV. In regions labeled by two letters (AB,AC,BD,...), we have costability of two different attractors.

The linear analysis of stability of the disordered state can be performed as in Sec. III. To obtain the continuous ''paramagnetic'' transitions, it is enough to replace a_S by a_D in Eqs. (29) and (30) for the critical temperature of the previous case. The dynamical phase diagrams display the same generic features. For example, in Fig. 13 we present the dynamical phase diagram for $a_S=0$ and $a_A=\frac{3}{2}$ in the $T\times a_D$ plane (which is very similar to the phase diagram in the $T\times a_S$ plane, for $a_A=\frac{3}{2}$ and $a_D=0$, as shown in Fig. 4).

V. CONCLUSIONS

We have performed detailed calculations to obtain the dynamical phase diagrams associated with a class of very simple neural networks including asymmetric interactions. Although there is no detailed balance, we can write a master equation for the synchronous updating of the probabilities of the microscopic states. In the thermodynamic limit and away from saturation, we obtain a set of nonlinear difference equations for the time evolution of the macroscopic order parameters. The attractors of these equations correspond to the stationary solutions of the problem.

At high temperatures, there is only a trivial (paramagnetic) disordered stable fixed point. At lower levels of noise, besides the ordered (ferromagnetic) fixed points, there is a rich structure of locked regions (Arnold tongues) into different cycles, with characteristic winding numbers, depending on the parameters of the embedding matrix. We perform analytic calculations for the paramagnetic lines of continuous transitions. The behavior of the largest Lyapunov exponent is used to establish the transitions between the periodic structures. We give numerical evidence for the existence of devil's staircases, with a fractal character, in terms of the winding numbers. Although there are also aperiodic limit cycles, associated with a vanishing Lyapunov exponent, we have not been able to find chaotic attractors. For analogs of the ANNNI model on a Cayley tree [6] the appearance of chaotic attractors is related to costability regions between modulated structures with *distinct* wave numbers or between the (ferromagnetic) uniform ordered and the modulated phases. Thus, as Coolen and Sherrington [2] have obtained a discontinuous transition between the (uniform) Hopfield and the oscillating regions for a class of models with $p\geqslant 3$, we believe that the absence of chaotic attractors is a particular feature of the $p=2$ case, where the dynamical transitions are always continuous.

We show that Farey numbers can be used to account for the appearance of the oscillating structures. In some regions of the dynamical phase diagrams, the coexistence of two distinct Farey structures gives rise to the overlap of several Arnold tongues (corresponding to the costability of two different periodic stationary states, with the same winding numbers but different structures).

It should be emphasized that the complex structure of the dynamical phase diagrams comes from the competition between symmetric and nonsymmetric contributions to the embedding matrix. As we have already remarked, there is a striking mathematical analogy with the phase diagram of the ANNNI model for helimagnetism (and, in particular, with some analogs of the ANNNI model on a Cayley tree [6]). We hope to have provided some illustrations of the complex effects of competing interactions. Also, we remark that our phase diagrams describe the behavior of two coupled neurons frequently considered in the literature [19,20]. As an application of these investigations, some simple networks, with just a few neuronal units, could certainly be built to take care of the generation of temporal sequences [8].

ACKNOWLEDGMENTS

We acknowledge the financial support of the Brazilian agencies CNPq and FAPESP.

[1] A. C. C. Coolen and Th. W. Ruijgrok, Phys. Rev. A **38**, 4253 (1988).

[2] A. C. C. Coolen and D. Sherrington, J. Phys. A **25**, 5493 (1992).

[3] S. N. Laughton and A. C. C. Coolen, J. Phys. A **27**, 8011 (1994).

[4] S. N. Laughton and A. C. C. Coolen, Phys. Rev. E **51**, 2581 (1995).

[5] W. Selke, Phys. Rep. **170**, 213 (1988); J. M. Yeomans, in *Solid State Physics*, edited by H. Ehrenreich and D. Turnbull (Academic, San Diego, 1988), Vol. 41, p. 151; W. Selke, in *Phase Transitions and Critical Phenomena*, edited by C. Domb and J. L. Lebowitz (Academic, New York, 1992), Vol. 15, Ch. 1, p. 1.

[6] C. S. O. Yokoi, M. J. Oliveira, and S. R. Salinas, Phys. Rev. Lett. **54**, 163 (1985); J. G. Moreira and S. R. Salinas, Phys. Rev. B **47**, 778 (1993); M. H. R. Tragtenberg and C. S. O. Yokoi, Phys. Rev. E **52**, 2187 (1995).

[7] E. Eisenstein, I. Kanter, D. A. Kessler, and W. Kinzel, Phys. Rev. Lett. **74**, 6 (1995); I. Kanter, D. A. Kessler, A. Priel, and E. Eisenstein, *ibid.* **75**, 2614 (1995).

[8] P. Peretto, *An Introduction to the Modeling of Neural Networks*, Collection Alia-Saclay: Monographs and Texts in Statistical Physics 2 (Cambridge University Press, Cambridge, 1992), p. 94.

[9] W. A. Little, Math. Biosci **19**, 101 (1974).

[10] W. A. Little and G. L. Shaw, Math. Biosci. **39**, 281 (1978).

[11] J. J. Hopfield, Proc. Natl. Acad. Sci. U.S.A. **79**, 2554 (1982).

[12] D. J. Amit, H. Gutfreund, and H. Sompolinsky, Phys. Rev. A **32**, 1007 (1985).

[13] D. J. Amit, H. Gutfreund, and H. Sompolinsky, Phys. Rev. Lett. **55**, 1530 (1985); Ann. Phys. (N.Y.) **173**, 30 (1987).

[14] M. Shiino, H. Nishimori, and M. Ono, J. Phys. Soc. Jpn. **58**, 763 (1989); H. Nishimori, T. Nakamura, and M. Shiino. Phys. Rev. A **41**, 3346 (1990).

[15] J. L. van Hemmen, Phys. Rev. Lett. **49**, 409 (1982).

[16] P. Peretto, Biol. Cybern. **50**, 51 (1984).

[17] D. C. Mattis, Phys. Lett. **56A**, 421 (1976).

[18] P. Peretto, J. Phys. **49**, 711 (1988).

[19] F. Pasemann and E. Nelle, in *Dynamical Systems—Theory and Applications*, edited by S. I. Andersson, A. E. Andersson, and U. Ottoson (World Scientific, Singapore, 1993), p. 167.

[20] N. Stollenwerk and F. Pasemann, Int. J. Bifurcation Chaos Appl. Sci. Eng. **6**, 693 (1996).

[21] J. Guckenheimer and P. Holmes, *Nonlinear Oscillations, Dynamical Systems, and Bifurcations of Vector Fields*, corrected 2nd printing (Springer-Verlag, New York, 1986).

[22] K. E. Bassler and R. B. Griffiths, Phys. Rev. B **49**, 904 (1994).

[23] G. Perez, S. Sinha, and H. A. Cerdeira, Europhys. Lett. **16**, 635 (1991).